AIAA JOURNAL
Vol. 39, No. 11, November 2001

Effective Test Time Evaluation in High-Enthalpy Expansion Tube

Akihiro Sasoh,* Yasuyuki Ohnishi,† Djameel Ramjaun,‡ and Kazuyoshi Takayama§
Tohoku University, Sendai 980-8577, Japan
Hirotaka Otsu¶
Shizuoka University, Hamamatsu 432-8561, Japan
and
Takashi Abe**
Institute of Space and Astronautical Science, Sagamihara 229-8510, Japan

Flow characterization experiments of stagnation enthalpies up to 37 MJ/kg are carried out in the recently commissioned expansion tube facility. The features and the effective duration time of the test flowfield are determined not only from static and pitot pressures but also by observing the temporal variation of radiating emission from a shock layer around a spherical forebody. The thickness of the radiating layer matches well with the numerical results. The arrival time of the contact surface between the acceleration and test gases is better identified both as a decrease in the radiating layer thickness and from the emission spectroscopy. The useful test time is determined by integrating the mentioned measurements.

Introduction

SUPERORBITAL reentry space experiments involving blunt-body capsule release from the H-II rocket proposed by the Institute of Space and Astronautical Science (ISAS), in collaboration with the Ministry of International Trade and Industry and National Space Development Agency (NASDA), Japan, has been scheduled for launch during 2001.[1] A sample return mission MUSES-C to an asteroid, proposed by ISAS, is also scheduled for launch in the year 2002.[2,3] During the reentry phase, the MUSES-C capsule will experience severe convective and radiative heat transfer at super orbital velocities above 11.5 km/s. The planned flight path of the reentry capsule is shown in Fig. 1 along with the operational regimes of conventional hypervelocity fluid dynamics test facilities. A considerable amount of high-quality experimental heat transfer data in high-enthalpy environment are needed for validating computational codes used in the design of the thermal protection system for the reentry capsule. However, there are very few impulsive test facilities capable of generating reliable hypervelocity flow around bodies in laboratory conditions. In the 1960s, NASA Ames Research Center built a ballistic range, which was combined with a shock tunnel for generating a counterflow against the projectile motion to carry out reentry aerothermodynamic experiments.[4] Although this facility would be suitable for a superorbital reentry aerodynamics study, it is very expensive, and synchronization of operation is rather difficult. On the other hand, an arc-driven wind tunnel capable of generating high-enthalpy flows has rather limited particle velocity simulation capability.[5] In a free-piston-driven shock tunnel, because of the complex hypersonic nozzle expansion flow problems coupled with melting of nozzle wall material, the stagnation enthalpy practically attainable is limited to about 25 MJ/kg (Refs. 6 and 7).

However, an expansion tube[8,9] is capable of generating high enthalpies over 25 MJ/kg. Recently, experiments in superorbital enthalpy conditions using an expansion tube have been reported.[10] Both convective and radiative heat transfer over bodies can be simulated in an expansion tube, with operational costs comparable to that of a shock tunnel.[11–13] However, one of the major limitations of the expansion tube operation is the reduced useful test times due to the governing unsteady fluid expansion. Figure 2 shows the typical x–t (distance vs time) diagram for a free-piston-driven expansion tube. The driver gas (DG) is compressed by the free piston in the compression tube (CT). On rupture of the primary diaphragm, a strong shock wave (SW1) propagates through the test gas (TG) filled in the shock tube (ST), subsequently impinging on the secondary diaphragm. Following the rupture of the secondary diaphragm, the shock wave (SW2) as a transmitted wave travels through the acceleration tube (AT), compressing the acceleration gas (AG) at low pressure. Reflected expansion waves in turn propagate through the TG, which further expands freely to an ultrahigh velocity of interest. In the increased enthalpy level, most of these processes involve nonequilibrium effects in AG and noninstantaneous diaphragm rupture. It is difficult to quantify accurately the test times using only conventional techniques such as pitot pressure measurements.

In the backdrop of concomitant needs of high-enthalpy facility to meet domestic demands, recently a free-piston-driven expansion tube facility, JX1, has been commissioned at the Shock Wave Research Center, Institute of Fluid Science, Tohoku University, Japan. In the test flow characterization of this study, the identification of the useful test time duration is stressed by employing both high-speed photography and emission spectroscopic techniques. The comparison between the measured and numerically simulated test flow conditions is also discussed.

Experimental Apparatus

Figure 3 shows the expansion tube JX1. It consists of a free-piston driver, ST, AT, and test/dump chamber. The reservoir has an inner diameter of 250 mm and a length of 1 m. The inner diameter and length of the CT are 150 mm and 3.0 m, respectively. The 7.0-kg free piston is made of aluminum alloy. Between the CT and ST, a layer of 1.6-mm-thick, mild steel primary diaphragm is inserted. The rupture pressure of the diaphragm is controlled by the depth of the cross grooves machined on its surface. The static rupture pressure is calibrated using a hydraulic test device. The inner diameter of both ST and AT is 50 mm. Before filling the AG, the AT and the test/dump chamber are evacuated using a turbomolecular vacuum pump down to 3×10^{-2} Pa.

Nine piezoelectric pressure transducers (PCB 113A03 or 112A21), four in the ST and five in the AT, are flush mounted on their inner surfaces. The rise time of all of the pressure transducers

Received 8 August 2000; revision received 9 April 2001; accepted for publication 9 April 2001.

*Associate Professor, Shock Wave Research Center, Institute of Fluid Science, 2-1-1 Katahira, Aoba-ku. Associate Fellow AIAA.

†Graduate Student, Shock Wave Research Center, Institute of Fluid Science, 2-1-1 Katahira, Aoba-ku.

‡Senior Researcher, Shock Wave Research Center, Institute of Fluid Science, 2-1-1 Katahira, Aoba-ku.

§Director, Professor, Shock Wave Research Center, Institute of Fluid Science, 2-1-1 Katahira, Aoba-ku. Senior Member AIAA.

¶Research Associate, Faculty of Engineering, 3-5-1 Jyohoku.

**Professor, Research Division for Space Transportation, 3-1-1 Yoshinodai. Member AIAA.

is 1 μs. The shock speed is determined by the method of time of flight over the separation distance between adjacent transducers.

The pitot pressure is measured 5 mm downstream from the exit of the AT. The structure of the pitot probe is similar to that is reported in Ref. 12. The piezoelectric pressure transducer (PCB113A03) is housed inside a 0.8-mm-diam hole drilled at the tip of the pitot probe. The transducer is protected by a metal disk against possible damage by direct impingement of high-enthalpy flows. Six off-axis perforations are machined on the disk to equilibrate the pressure through the disk.

The measured signals are transiently recorded in a digital memory (DL716; Yokogawa) and are analyzed using a personal computer.

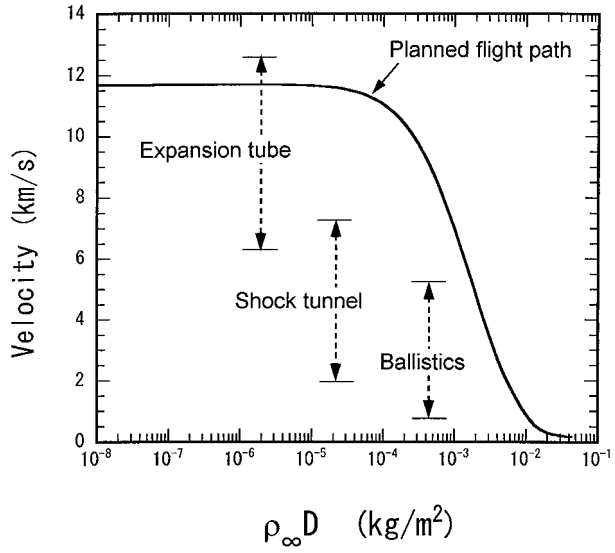

Fig. 1 Planned reentry condition of MUSES-C capsule: arrow indicates typical velocity regime of ground test facilities, ρ_∞ is freestream density, and D is capsule diameter.

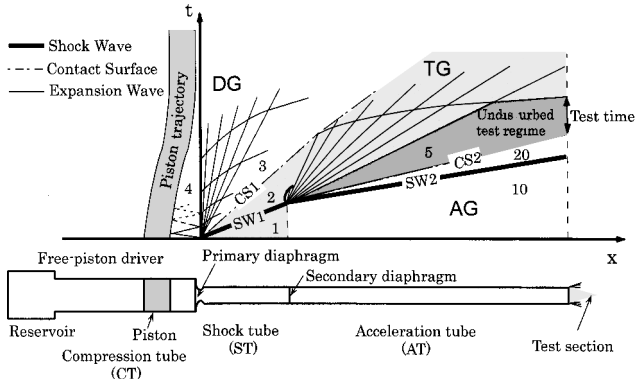

Fig. 2 Typical x–t (distance–time) diagram of free-piston-driven expansion tube operation.

Driver Operation Design

The free-piston driver is designed by revising the tuned operation criteria of Ito et al.[14] They proposed 1) the soft landing criterion and 2) the holding time criterion for designing the free-piston driver. The former is a condition for the free piston not to collide against the end wall of the compression tube with a velocity exceeding a critical value. Because facility damage due to the collision becomes crucial, this criterion is adopted in the present study. However, the latter one is not adopted in the present study because the test time in an expansion tube is not necessarily directly related with the holding time of the free-piston driver. Rather, the test time, in principle, is determined from the nonlinear wave interactions occurring in the test gas slug.[15]

The unsteady, one-dimensional compressible flow solver originally developed for designing the High-Enthalpy Shock Tunnel (HI-EST), Kakuda Research Center, National Aerospace Laboratory, Kakuda, Japan,[16] is used with appropriate modifications for numerically simulating the free-piston-driver operation. In the numerical simulation, to specify the criterion for the soft landing, the residual velocity of the piston colliding against the CT end wall is assumed to be lower than 10 m/s. The compression ratio for primary diaphragm rupture is 20 ± 0.4. The operation condition of the free-piston driver is kept unchanged in the present study.

Evaluation of Stagnation Enthalpy

Typical operation conditions of the expansion tube are given in Table 1. The stagnation enthalpy of the test flow is varied by varying the fill pressure of the AG. Except for the spectroscopic measurement, which will be described later, dry air is used as the test gas in all of the experiments.

In Table 2, measured and estimated test flow parameters are given. The shock speed is determined by monitoring the static pressures, p_8 and p_9, measured at 0.680 m and 0.015 from the AT exit, respectively.

The test flow parameters given in Table 2 are calculated using a computer program assuming for equilibrium flow.[17] The velocity of CS2, the contact surface between the acceleration gas and the test gas (Fig. 2), is assumed to be equal to the particle velocity behind SW2. The computation is iteratively carried out until all of the relations mentioned earlier are satisfied for a given temperature. The stagnation enthalpies in the present experiments are estimated to be 31 and 37 MJ/kg in cases A and B, respectively.

Table 1 Expansion tube operation conditions

Component	Parameter	Value[a]	Material/species
Resevoir	Fill pressure	2.6 MPa	Dry air
CT	Fill pressure	118 kPa	He (DG)
Primary diaphragm	Static rupture pressure	20 MPa	Mild steel
ST	Fill pressure	3.5 kPa	Air or (80%N_2 + 20%O_2) (TG)
Secondary diaphragm	Thickness	17 μm	Cellophane
AT	Fill pressure	Case A: 16 Pa Case B: 3.5 Pa	Dry air (AG) Dry air (AG)

[a]Pressures are of an absolute value.

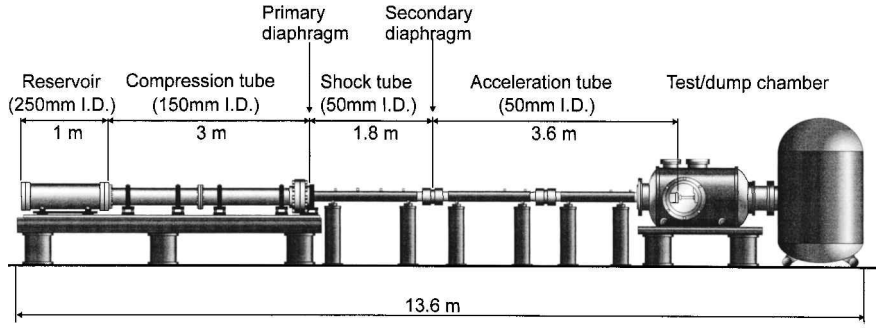

Fig. 3 Schematic of expansion tube, JX-1

Table 2 Measured freestream characteristics of test flows

Variable	Case A	Case B	Source
SW2 speed, km/s	7.9 ± 0.1	8.9 ± 0.1	Measured (time of flight)
Static pressure, kPa	9.7 ± 1.2	2.9 ± 0.5	Measured
Pitot pressure, kPa	800 ± 50	670 ± 13	Measured
Mass-averaged particle velocity, km/s	7.5 ± 0.1	8.5 ± 0.1	Calculated[a]
Temperature, K	2300 ± 400	1050 ± 200	Calculated[a]
Density, kg/m^3	1.2×10^{-2}	8.2×10^{-3}	Calculated[a]
Flow Mach number	8.4 ± 0.6	13.5 ± 1.2	Calculated[a]
Stagnation enthalpy, MJ/kg	31 ± 0.9	37 ± 0.2	Calculated[a]

[a]Calculated for one-dimensional, inviscid, equilibrium flow.[17]

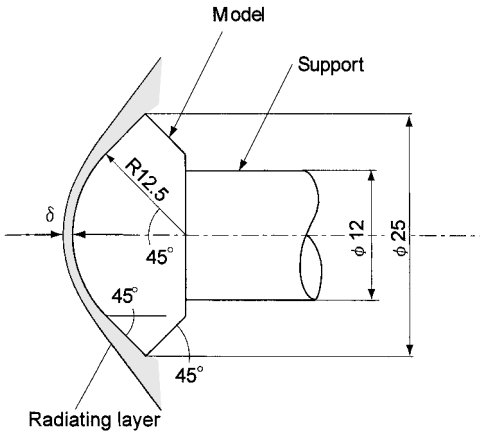

Fig. 4 Muses-C reentry capsule model.

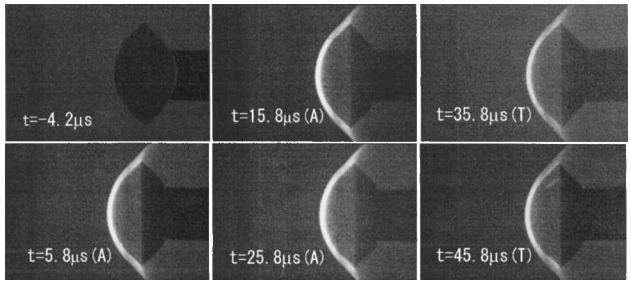

a) Case A

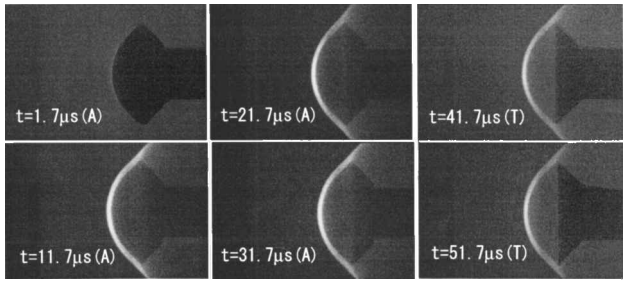

b) Case B

Fig. 5 Framing photographs of radiating layer over the blunt body; frame interval equals 10 μs; time t measured from the SW2 arrival, A indicates AG, and T indicates TG.

Radiation over a Blunt Body

Figure 4 shows the $\frac{1}{16}$-scaled model of the MUSES-C reentry capsule used in the study. The forebody comprises a sphere and a truncated cone with 45-deg apex angle. It is made of stainless steel (SUS 304). Supported by an 12-mm-diam brass rod, the tip of the model is located 2 mm downstream of the acceleration tube exit. In the present study, the test flow Mach number is at least 8.3, and the corresponding Mach angle is 6.9 deg, engulfing the model within the inverse Mach cone generated from the AT exit peripheral.

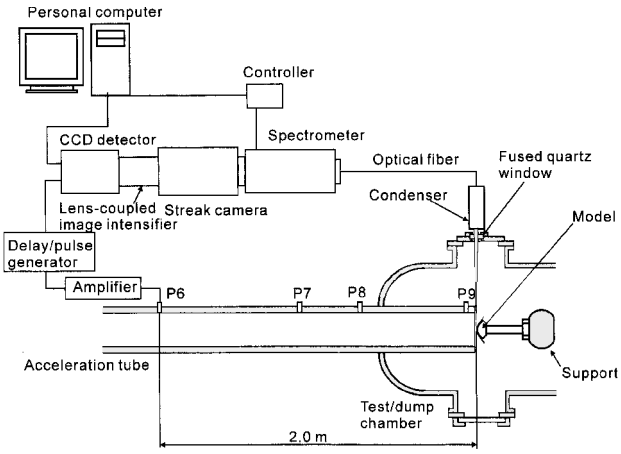

Fig. 6 Experimental setup of streak spectroscopy.

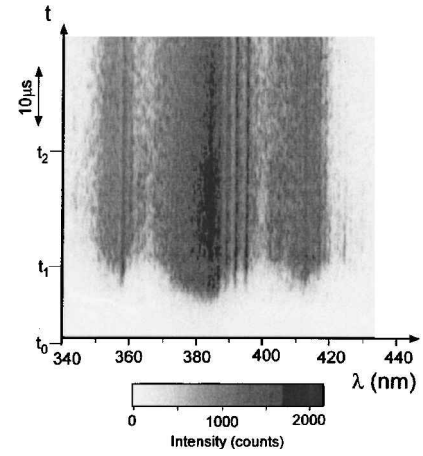

a) Case A

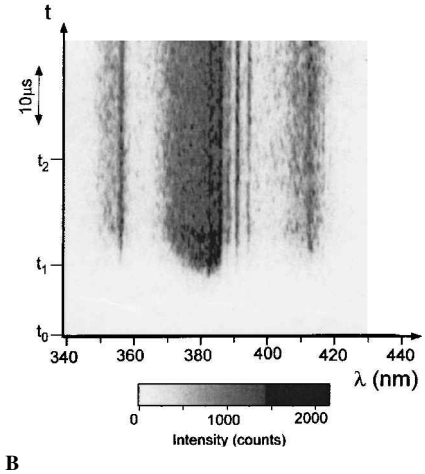

b) Case B

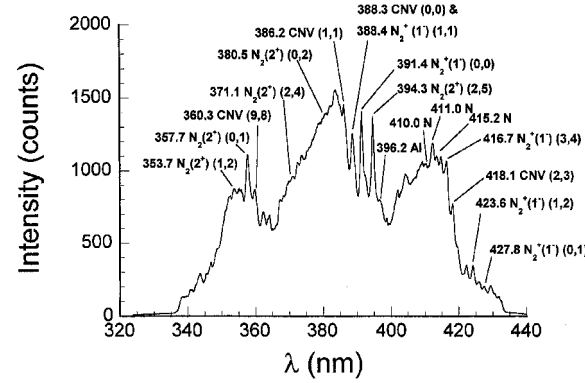

c) Time-integrated intensity, case A

Fig. 7 Intensity contours of streak spectroscopy.

Framing Photography of Radiating Layer

The radiating shock layer surrounding the forebody is visualized using a high-speed image converter camera (IMACON 468; Headland Photonics). Six frames are sequentially recorded in a single shot. Each frame has 576 × 385 pixel resolution. The exposure time is adjusted to 200 ns in each frame. The framing interval is varied from 5 to 32 μs. A Xe flush light with 500-μs pulse duration is used to backlight the model. The system is triggered by the signal of p_6 located 2 m upstream of the AT exit.

Figure 5a and 5b show sequential photographs of the radiating layer observed around the model. In Fig. 5b, the first four frames correspond to the passage of the AG and the last two to the test gas. In the first frame, the primary shock wave has just reflected from the model and a quasi-steady-state flow has not been established. From the second to fourth frames, a quasi-steady-state flow of the AG is barely established. The visualized thickness of the radiating layer on the stagnation line is designated by δ (Fig. 4). In the fifth and sixth frames, during the TG passage, δ slightly decreases. This decrease is caused by an increase in the flow Mach number; based on equilibrium speed of sound, in case A (B) the flow Mach number of the AG and TG equal 3.8(3.3) and 8.4(13.5), respectively. When it is considered that the images are the side view of the axisymmetric flow, the intensity of the radiation near the stagnation point, where the physical thickness is small, is strongest. The earlier mentioned variation of δ is observed also in Fig. 5a. Good agreements are obtained between the experiment and the numerical simulation both on the value of δ and the bow SW shape. (We are preparing to publish the numerical simulation results.) The time variation analysis of δ is discussed while describing the integrated evaluation of test time.

Streak Emission Spectroscopy

Figure 6 shows the setup used for emission spectroscopy measurement. The emitted radiation is captured through the window made of fused quartz, the condenser, and the optical fiber to the streak spectrometer. The focal point is set in the radiating layer near the stagnation point. Because the thickness of the radiating layer on the stagnation line is of the order of 0.9 mm, the measured spectroscopic data cannot be spatially resolved in the shock layer. The monochromator (SP-408I; Acton Research Company) has a focal length of 500 mm. The blaze wavelength of the grating is 500 nm.

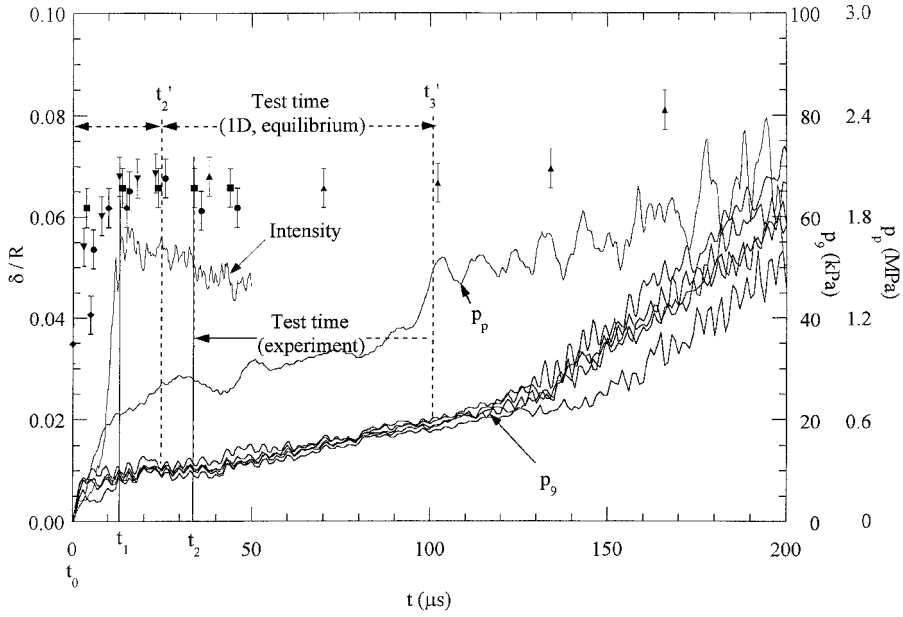

a) Case A

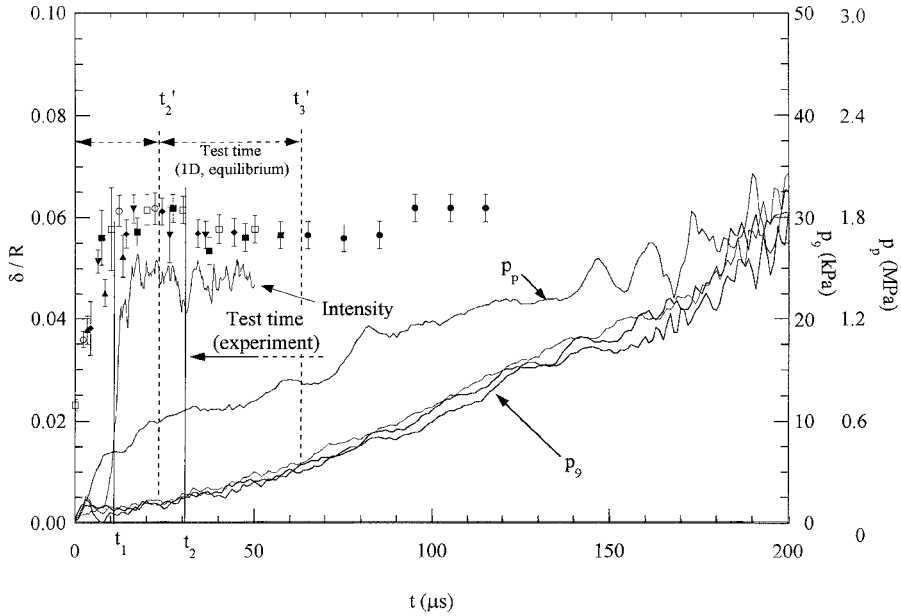

b) Case B

Fig. 8 Time variations of static pressure p_9, pitot pressure, radiation intensity (in arbitrary unit), and the thickness of radiating layer on the stagnation line.

The number of grooves per millimeter is varied from 150 to 1200. The spectrograph is imaged onto the streak camera (C2830; Hamamatsu Photonics) and then onto a lens-coupled image intensifier (LCI-10; EG&G Princeton Applied Research) and finally recorded on a cryogenically cooled charge-coupled device (CCD) detector (1530-CUV-1024s; EG&G Princeton Applied Research). The CCD detector has 1024 (horizontal) × 256 (vertical) pixels with an 18-bit dynamic range. In this measurement, the horizontal axis corresponds to the wavelength and the vertical axis is to time.

In the spectroscopic experiments, 80% nitrogen and 20% oxygen (molar ratio) mixture is used as TG. Only AG (dry air) contains about 0.03% carbon dioxide, which can contribute to radiation from the shock layer due to the CN violet band. Figures 7a and 7b show contours of streak spectroscopic images in a wavelength range of 340–430 nm. Major radiating sources in this range are N_2^+ first negative band, N_2 second positive band, and CN violet band (Fig. 7c). The possible sources of the carbon are carbon dioxide contained in the AG, residual materials in ST, AT, and the test/dump section, and the secondary diaphragm material. Even after careful cleaning, the intensity of the CN violet could not be fully eliminated.

However, the existence of this band does not necessarily yield a negative effect. In the present study, the radiation of this band becomes useful for validating the estimation of the test time. As is obviously seen in Fig. 7a, the intensity of CN violet becomes highest between $t = t_1$ and t_2. The duration time synchronizes with the AG passage time, thereby decreasing the intensity during the useful test time.

In case B (Fig. 7b), the contrast in the intensity is not distinctly observed. The tendency is repeatedly observed during the experiments. A pit in the radiative intensity variation synchronized to CS2 passage. Currently, the reason for this result is not clear, and further study is mandatory.

Integrated Evaluation of Test Time

In Figs. 8a and 8b, the time variation of p_9, pitot pressure, radiative intensity, and δ are plotted. The time t is measured from the moment of the SW arrival at the stagnation point of the blunt body. The time for p_9 is shifted as if it is measured at the same axial position as that of the stagnation point. Also in Fig. 8, the duration times of the AG passage and of the test flow calculated from relations for one-dimensional, inviscid, equilibrium flow (see Table 2) are plotted.

The static pressure sharply rises with the response time of the pressure transducer. It keeps an almost constant value and then gradually increases. The time of this pressure increase appears much earlier than the arrival time of the expansion wave propagating as a leading left-running characteristic behind the test flow. The main cause of this pressure increase is believed to be growth of a boundary layer.[18,19]

In the variations of δ, distinct tendencies are seen in both cases. From $t = 0$ to t_1, δ rises sharply with corresponding increase in the radiation intensity. This duration time corresponds to the establishment of quasi-steady-state flow of the AG. From $t = t_1$ to t_2, δ is almost constant. Then, after $t = t_2$, it settles to a value lower by 5–8%. In case A, the radiative intensity drops, and in case B, a pit in the radiative intensity appears at $t = t_2$. The agreement on the timing of the transition between δ and the radiative intensity strongly suggests that the measured t_2 is the effective arrival time of CS2.

To evaluate the test time, available time windows of the measured parameters are summarized in Figs. 9a and 9b. The available time window is estimated from the variation of δ starting at $t = t_2$ and terminating when it starts to increase again. In case A, a distinct drop of the radiation intensity gives another starting criterion for the test flow. These two are close to each other. The time windows determined from p_9 and the pitot pressure depend on a tolerance for the deviation from their nominal values. As seen in Figs. 9a and 9b, if the tolerance is set to be 10% deviation, the test times become 22 μs in case A and 13 μs in case B, respectively.

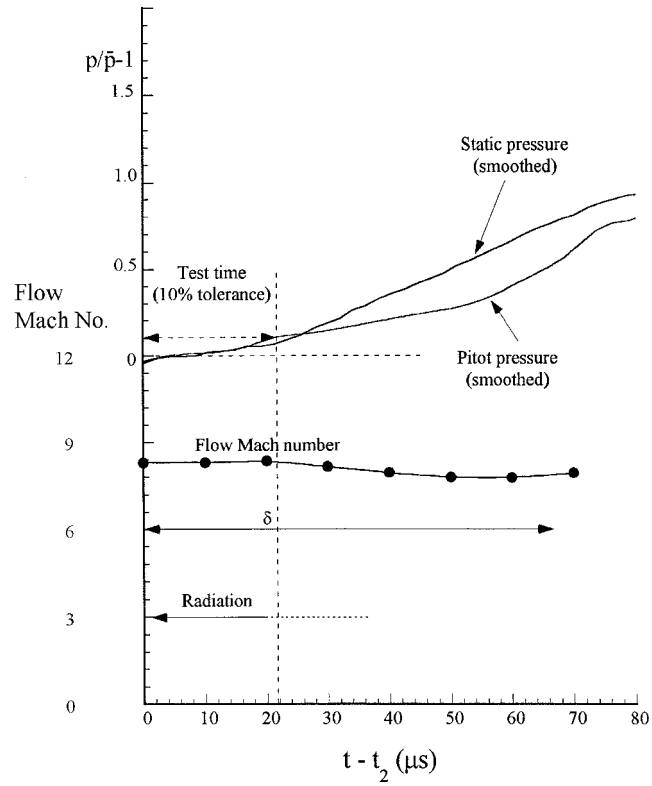

a) Case A

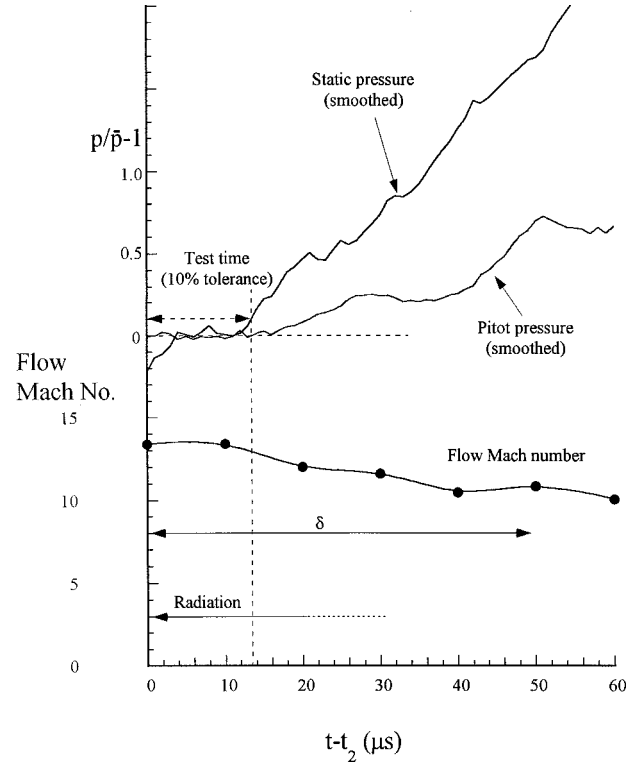

b) Case B

Fig. 9 Time chart for the determination of test time.

Discussion

Relation Between δ and Shock Standoff Distance

In the present paper, the thickness of the radiating layer, δ, has been treated as an important characteristic parameter. It is necessary for this parameter to be related with the shock standoff distance. Figure 10 shows the distributions of emission power along the stagnation line calculated using the radiation analysis package SPRADIAN, developed by ISAS[20] based on the results from our numerical simulation. In the numerical simulation, the upstream flow is assumed to contain only molecular nitrogen and oxygen. The two-temperature model of Park,[21] in which the heavy particle translational temperature equals the rotational temperature and the vibrational temperature equals the electron translational temperature,

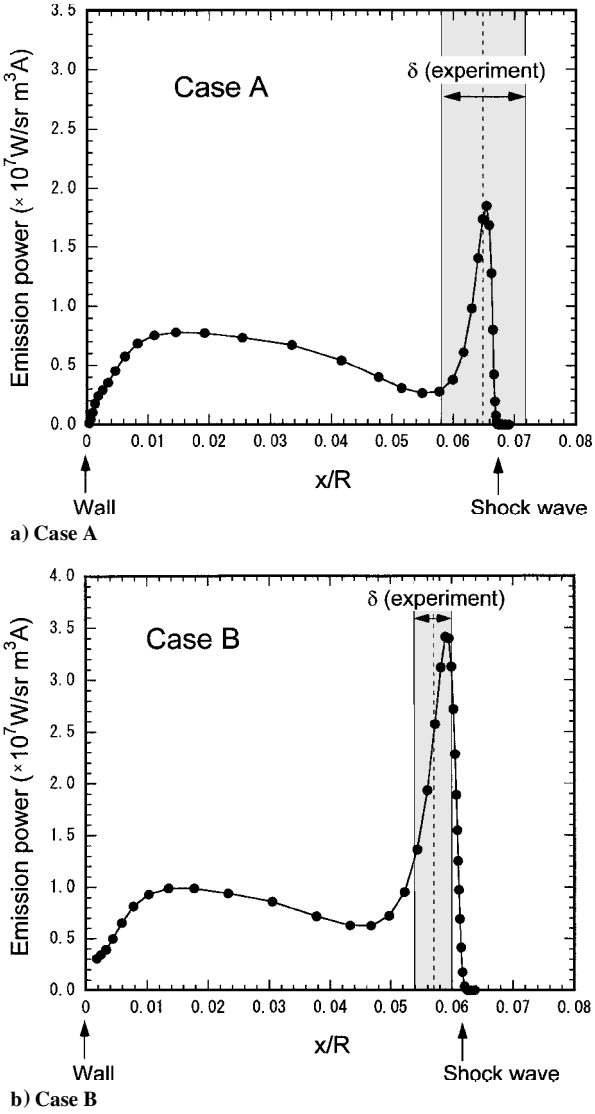

Fig. 10 Distribution of emission power along the stagnation line; flowfield is numerically simulated (results to be published). Emission power is calculated using SPRADIAN.

is employed. The dominant radiators in the shock layer are N_2^+ first negative band and N_2 second positive band. As seen in Fig. 10, the emission power becomes highest immediately behind the SW. At this location, the heavy particle translational–rotational temperature and the vibrational–electron translational temperature are not in equilibrium. Because of this nonequilibrium relation, the former overshoots, thereby producing the high emission power. Downstream of this nonequilibrium region, these temperatures become equilibrated, resulting in another peak in the emission power. The distance between the SW and the first peak of the emission power equals a relaxation length for the nonequilibrium radiation and is $3 \pm 1\%$ of the shock standoff distance. The outer boundary of the radiating layer observed in the experiment agrees well with the peak location obtained in the computations within the uncertainty in the image processing (shown as a gray zone in Figs. 10a and 10b).

It follows from the preceding discussion that on the stagnation line 1) the distance of the peak emission location from the wall is smaller than the shock standoff distance only by about 3% and 2) the measured value of δ agrees with the numerically simulated peak location within the uncertainty in the image processing. Therefore, it is reasonably concluded that δ approximately equals the shock standoff distance.

Possible Reason for Delay in Test Flow Arrival

From the discussion in the preceding section, it is clear that t_2 determined from the time variation of δ becomes the effective arrival time of the TG. However, this time differs by about 30% from the one-dimensional, inviscid, equilibrium estimation.

One of the possible reasons for this difference is the nonequilibrium effect of the AG. If the AG is assumed to be frozen with a specific heat ratio of 1.4, the calculated value of t_2 is 90 μs for case A and 79 μs for case B. Of course, such an assumption is far from the reality. The measured t_2 is much closer to that calculated, which assumes the equilibrium condition of the AG, as seen from in Figs. 8a and 8b. However, it is expected that at least partially the AG does not reach an equilibrium state. This can account for the mechanisms for the difference in the estimated CS2 arrival times.

Conclusions

In the present study, a test flow of 37 MJ/kg at a static pressure of 2.9 kPa is generated using the free-piston-driven expansion tube. The effective test time is estimated using static and pitot pressure measurements, high-speed photography, and time-resolved spectral emission measurements from the radiating shock layer around the blunt body. It is found that the arrival of the test gas is delayed by about 30% to the time estimated assuming chemical and thermal equilibrium for the AG. The estimated test time with an allowance of 10% error becomes 22 and 13 μs for stagnation enthalpies of 31 and 37 MJ/kg, respectively. Basic flow characteristics such as a shock standoff distance, shock layer shape, and the stagnation pressure under such nonequilibrium condition for the MUSES-C model have been measured and agree with the numerical results.

Acknowledgments

Special thanks are extended to Nac Company, Ltd., for providing the IMACON camera. The authors gratefully acknowledge valuable discussions on expansion tube operation and related diagnostics with R. G. Morgan of the Center for Hypersonics, Department of Mechanical Engineering, and T. J. McIntyre of the Department of Physics, University of Queensland, Brisbane, Australia. We acknowledge G. Jagadeesh of the Shock Wave Research Center for valuable discussions and his proofreading the paper. We appreciate valuable technical assistance from O. Onodera, H. Ojima, T. Owaga, K. Takahashi, T. Watanabe, M. Kato, and Y. Fushimi, of the Institute of Fluid Science, Tohoku University, and M. Kikuchi, graduate student of the Department of Aeronautical Engineering, Tohoku University.

References

[1]Morita, Y., Kawaguchi, J., Inatani, Y., and Abe, T., "Demonstrator of Atmospheric Reentry System with Hyperbolic Velocity—DASH," International Astronautical Federation, Rept. IAF-99-V.2.09, Oct. 1999.

[2]Kawaguchi, J., Fujiwara, A., and Sawai, S., "Sample and Return Mission from Asteroid Nereus via Solar Electric Propulsion," *Acta Astronautica*, Vol. 38, No. 2, 1996, pp. 87–101.

[3]Suzuki, K., Kubota, H., Fujita, K., and Abe, T., "Chemical Nonequilibrium Ablation Analysis of MUSES-C Superorbital Reentry Capsule," AIAA Paper 97-2481, June 1997.

[4]Carros, R. J., and DeRose, C. E., "Counterflow Facilities," *Ballistic Range Technology*, AGARDograph, Rept. 138, 1970, Chap. 5.

[5]Park, C., *Nonequilibrium Hypersonic Aerothermodynamics,* Wiley, New York, 1990, Chap. 7.

[6]Hanemann, K., Reimann, B., and Schnieder, M., "Combined Experimental and Numerical Characterisation of HEG Test Section Flow," *Proceedings of the 22nd International Symposium on Shock Waves*, Univ. of Southampton, Southampton, England, U.K., 2000, pp. 453–458.

[7]Itoh, K., Takiguchi, M., Komuro, T., Sato, K., Tanno, H., Ueda, S., Narita, T., and Maehara, T., "Effect of Throat Melting on Nozzle Flow Characteristics in an High Enthaply Shock Tunnel," *Proceedings of the 22nd International Symposium on Shock Waves*, Univ. of Southampton, Southampton, England, U.K., 2000, pp. 459–464.

[8]Resler, E. L., and Blossom, D. E., "Very High Mach Number Flows by Unsteady Flow Principles," School of Aeronautical Engineering Monograph, Cornell Univ., Ithaca, NY, Jan. 1952.

[9]Trimpi, R. L., "A Preliminary Technical Study of the Expansion Tube, A New Device for Producing High-Enthalpy Short-Duration Hypersonic Gas Flows," NASA R-133, 1962.

[10]Morgan, R. G., "Superorbital Expansion Tube," *Proceedings of 21st International Symposium on Shock Waves*, Vol. 1, Panther, Fyshwick, Australian Capital Territory, Australia, 1998, pp. 71–76.

[11]Palmer, R. A., Hannemann, K., and Morgan, R. G., " Experimental and Numerical Blunt Body Heat Transfer in an Expansion Tube," *Proceedings of*

21st International Symposium on Shock Waves, Vol. 1, Panther, Fyshwick, Australian Capital Territory, Australia, 1998, pp. 703–708.

[12]Neely, A. J., Stalker, R. J., and Paull, A., "High Enthalpy, Hypervelocity Flows of Air and Argon in an Expansion Tube," *Aeronautical Journal*, Vol. 95, June/July 1991, pp. 175–186.

[13]Calleja, J., and Tamagno, J., "Calibration of HYPULSE for Hypervelocity Air Flows Corresponding to Flight Mach Numbers 13.5, 15 and 17," NASA CR-191578, Dec. 1993.

[14]Ito, K., Ueda, S., Komuro, T., Sato, K., Takahashi, M., Miyajima, H., Tanno, H., and Muramoto, H., " Improvement of a Free Piston Driver for a High-Enthalpy Shock Tunnel," *Shock Waves*, Vol. 8, No. 4, 1998, pp. 215–233.

[15]Paull, A., and Stalker, R. J., "Test Flow Disturbances in an Expansion Tube," *Journal of Fluid Mechanics*, Vol. 245, 1992, pp. 493–521.

[16]Tani, K., Itoh, K., Takahashi, M., Tanno, H., Komuro, T., and Miyajima, H., "Numerical Study of Free-Piston Shock Tunnel Performance," *Shock Waves*, Vol. 3, No. 4, 1994, pp. 313–319.

[17]Heiser, W. H., and Pratt, D. T., *Hypersonic Airbreathing Propulsion*, AIAA Education Series, AIAA, Washington, DC, 1994 (attached computer program).

[18]Mirels, H., "Test Time in Low-Pressure Shock Tubes," *Physics of Fluids*, Vol. 6, No. 9, 1963, pp. 1201–1214.

[19]Jacobs, P. A., "Numerical Simulation of Transient Hypervelocity Flow in an Expansion Tube," *Computers Fluids*, Vol. 23, No. 1, 1994, pp. 77–101.

[20]Fujita, K., and Abe, T., "SPRADIAN, Structured Package for Radiation Analysis: Theory and Application," Inst. of Space and Astronautical Science, ISAS Rept. 669, Kanagawa, Japan, Sept. 1997.

[21]Park, C., "Assessment of Two-Temperature Kinetic Model for Ionizing Air," AIAA Paper 87-1574, 1987.

J. P. Gore
Associate Editor